

# Decadal modulation of East China winter precipitation by ENSO

Jia Liu<sup>1</sup> · Hui Wang<sup>2</sup> · Er Lu<sup>1</sup>  · Arun Kumar<sup>2</sup>

Received: 9 June 2016 / Accepted: 26 October 2016  
© Springer-Verlag Berlin Heidelberg 2016

**Abstract** The decadal modulation of East China winter precipitation by the El Niño–Southern Oscillation (ENSO) is examined using both observational data and coupled global climate model simulations. The co-variability between 68-year (1948–2015) observed East China precipitation and tropical Pacific sea surface temperature (SST) is quantified by the singular value decomposition (SVD) method. The first SVD mode relates Southeast China winter pluvial (drought) to the tropical Pacific El Niño (La Niña) SST. A comparison between two 480-year model simulations with and without ENSO suggests that ENSO can modulate both the intensity and frequency of East China winter precipitation. In the presence of ENSO, maximum precipitation anomalies over Southeast China can be increased by 50% and largely on the interannual timescale

(3–6 years). It is also demonstrated that there is an asymmetry in the precipitation and circulation responses to warm and cold phases of ENSO. The responses are sensitive to the intensity of SST anomalies during El Niño, but less sensitive to SSTs during La Niña. This sensitivity, together with the decadal variations of ENSO, helps understand the observed decadal changes in the strength of the association between wintertime tropical Pacific SST and East China precipitation. The association is relatively weak during 1948–1977 when La Niña occurred more frequently, but strong during 1978–1999 when El Niño occurred more frequently. In the last 16 years (2000–2015) the association is weakest, likely due to the weakened variability of tropical Pacific SST since 2000.

**Keywords** Precipitation · ENSO · East China · Interdecadal variability

---

This paper is a contribution to the special collection on ENSO Diversity. The special collection aims at improving understanding of the origin, evolution, and impacts of ENSO events that differ in amplitude and spatial patterns, in both observational and modeling contexts, and in the current as well as future climate scenarios.

---

This special collection is coordinated by Antonietta Capotondi, Eric Guilyardi, Ben Kirtman and Sang-Wook Yeh.

---

✉ Er Lu  
elu@nuist.edu.cn

<sup>1</sup> Key Laboratory of Meteorological Disaster, Ministry of Education (KLME) / Joint International Research Laboratory of Climate and Environment Change (ILCEC) / Collaborative Innovation Center on Forecast and Evaluation of Meteorological Disasters (CIC-FEMD), Nanjing University of Information Science and Technology, Nanjing 210044, Jiangsu, China

<sup>2</sup> NOAA/NWS/NCEP/Climate Prediction Center, College Park, MD 20740, USA

## 1 Introduction

Observational data show that the climate in China has experienced significant changes in recent decades (Chen et al. 2004). Coincident with these changes, there are also prominent interannual and interdecadal variations in both the atmosphere and ocean, such as precipitation over China and sea surface temperature (SST) in the Pacific Ocean. A better understanding of the interannual and interdecadal variations is important to the interpretation and for the perception of the climate trend in China, as well as the long-term development plans of the national economy (Li et al. 2004).

The El Niño–Southern Oscillation (ENSO) is the strongest interannual air–sea coupled mode in the tropics. It is also the most important source of the interannual variability

in the global climate system. Through the atmospheric teleconnection, ENSO strongly affects precipitation in China. A large number of studies reveal a close relationship between ENSO and China precipitation on the interannual timescale (e.g., Chen et al. 2012; He et al. 2013; Zhou et al. 2010; Zong et al. 2010). Co-variations of El Niño/La Niña and South China winter precipitation on the decadal timescale are also observed (Yuan et al. 2014).

The Pacific-East Asian teleconnection, a circulation pattern that links central tropical Pacific SST anomalies with East Asian climate variations, has been proposed to be responsible for the connection between ENSO and China precipitation (Wang et al. 2000). It is suggested that the key system that links the equatorial central Pacific warming (cooling) and weak (strong) East Asian winter monsoon is the large-scale anomalous anticyclone (cyclone) over the western North Pacific.

Most of the previous studies have focused on the relationship between ENSO and summer precipitation in China, (e.g., Zong et al. 2010; Feng and Hu 2004). For example, in El Niño (La Niña) years, summer precipitation in the Yangtze River Basin and to the south tends to be above (below) normal (Ye 1988; Jin and Tao 1999). Although winter precipitation is generally less as compared to summer, but due to low temperatures in wintertime, winter precipitation anomalies can lead to severe winter disasters. Winter precipitation may also lead to severe damage to property and plants (Feng et al. 1985).

In the context of global climate change, the regional climate change in East China is significant, which has a great influence on people's life (Gao et al. 2008; Wang et al. 2008). It is also important to understand to what extent the climate trends are modulated by low-frequency variability, for example, decadal variation. This is because modulation of trends by low-frequency variability has important implications, both from the perspective of near term planning and in the context of perceptions about the climate change.

The increasing occurrence of extreme winter events has brought more attention to the decadal variability of winter precipitation and has raised various questions. In particular, what is the mechanism of the decadal variations in winter precipitation, and further, can it be related to other facets of climate variability, such as ENSO? Does the relationship between East China precipitation and ENSO depend on the state of ENSO? More specifically, how are the responses of precipitation (and the related atmospheric circulation) to ENSO SSTs sensitive to the phase and intensity of ENSO?

In this study, we aim to analyze the decadal modulation of East China winter precipitation by ENSO. Wang and Kumar (2015) demonstrated that a modeling approach through a comparison between two simulations with and without ENSO is an effective way in assessing the impact of ENSO on the Southwest U.S. precipitation. Here we use

the same methodology to study the influence of ENSO on the East China precipitation. Through the analysis of East China winter precipitation (and the related atmospheric circulation) in response to ENSO, we expect to reveal the sensitivity of the responses to the ENSO phase and intensity, which may help us better understand the observed decadal variations of winter precipitation in East China.

## 2 Data, model, and methods

### 2.1 Data

The data used in this study include both observations and model simulations. The observational data consist of monthly mean precipitation, SST, and 200-hPa geopotential height from 1948 to 2015. The precipitation is from the National Oceanic and Atmospheric Administration (NOAA) Precipitation Reconstruction over Land (PREC/L) dataset (Chen et al. 2002) with a spatial resolution of  $1^\circ \times 1^\circ$  longitude  $\times$  latitude (data available at <http://www.esrl.noaa.gov/psd/data/gridded/data.precl.html>). The SST is from the NOAA Extended Reconstructed SST (ERSST) dataset, version 3b (Smith et al. 2008) with a  $2^\circ \times 2^\circ$  resolution (available at <http://www.esrl.noaa.gov/psd/data/gridded/data.noaa.ersst.html>). The 200-hPa height is from the National Centers for Environmental Prediction-National Center for Atmospheric Research (NCEP-NCAR) Reanalysis product (Kalnay et al. 1996) having a resolution of  $2.5^\circ \times 2.5^\circ$ . The same variables are also taken from the model simulations described below.

### 2.2 Model

The model employed in this study is the NCEP Climate Forecast System (CFS) version 1 (Saha et al. 2006). It is a fully coupled ocean-land-atmosphere dynamical seasonal prediction system, which became operational at NCEP in 2004. The atmospheric component of the CFS is a low-resolution (T62) version of the Global Forecast System (GFS; Moorthi et al. 2001) that was the operational global weather prediction model at NCEP starting in 2003. The ocean component is the Geophysical Fluid Dynamics Laboratory (GFDL) Modular Ocean Model version 3 (MOM3; Pacanowski and Griffies 1998). There are many studies using CFS model data and analyzing the interannual variations of precipitation and the large-scale circulation associated with the Asian monsoon (e.g., Yang et al. 2008; Chen et al. 2010).

In order to explore the effects of ENSO on climate variability, we use two 500-year simulations. One is a free coupled run with the ENSO variability (referred to as an ENSO run), and the other is a no-ENSO run in which the

model SST was nudged to the observed climatological SST seasonal cycle in the tropical Pacific (140°E–75°W, 10°S–10°N). This was done by substituting the model daily SST in this region with a new SST, which is a combination of the model SST and observed daily SST climatology. The weighting coefficient for the observed SST climatology is 1/3 over the tropical Pacific domain and linearly reduced to zero on the border of a larger domain (130°E–65°W, 15°S–15°N). More detailed descriptions of the model setup for the two runs can be found in Wang et al. (2012b). For both the ENSO run and no-ENSO run, the last 480 years of the simulations are analyzed in this study. The differences between the two model experiments elucidate the impacts of ENSO. This set of simulations has previously been analyzed to characterize the ENSO variability (Kim et al. 2012), the Pacific decadal oscillation (Wang et al. 2012a, b; Kumar et al. 2013), the Indian Ocean dipole (Wang et al. 2016), and the impact of ENSO on U.S. Southwest drought (Wang and Kumar 2015).

### 2.3 Methods

In this study, winter seasonal means are the averages of monthly data of January, February, and March (JFM). Although ENSO SST anomalies peak in December or January, it takes some time for the atmosphere to respond to the tropical heating associated with the ENSO SST and to establish a well-defined teleconnection pattern (Kumar and Hoerling 2003). Therefore, the typical extratropical winter precipitation pattern caused by ENSO mainly appears in JFM (e.g., Wang and Fu 2000).

The singular value decomposition (SVD) analysis (Bretherton et al. 1992) is applied to extract the coupled modes between winter (JFM) SST in the tropical Pacific and precipitation in East China. Considering the lagged response of extratropical precipitation to the ENSO SST, it would be more reasonable to perform an SVD analysis between December–January–February (DJF) tropical SST and JFM China precipitation. However, given strong persistence of tropical SST anomalies through the winter months, the results of the lagged SVD would not significantly differ from those presented in this paper based on both JFM SST and precipitation data. In order to show that the leading SVD mode represents the co-variations of the dominant modes of the variability in both SST and precipitation fields, the empirical orthogonal function (EOF) method is also used.

Correlation analyses are applied to illustrate the circulation response to the ENSO intensity. Composite analyses are also used to document different intensities of El Niño and La Niña SSTs and the typical precipitation anomalies associated with the different ENSO intensities. The

statistical significance of the correlation coefficients is determined by the two-tailed *t* test (Snedecor and Cochran 1989).

### 3 Climatology and variability of China winter precipitation

Figure 1a shows the observed long-term mean China winter (JFM) precipitation averaged from 1948 to 2015. A region with abundant precipitation is found in Southeast China with maximum precipitation exceeding 4 mm day<sup>-1</sup>. This wet region is associated with a rich moisture supply from the western North Pacific. The rest of the country is relatively dry in winter, receiving less than 1 mm day<sup>-1</sup> precipitation on average.

The climatology of China winter precipitation in the CFS is shown in Fig. 1b for the ENSO run and in Fig. 1c for the no-ENSO run, respectively. It is evident that there are positive mean biases of winter precipitation over the Northeast and central China in both the simulations. In spite of the biases, both model climatologies resemble the observed pattern (Fig. 1a) with large winter precipitation in the Southeast. It is also interesting to note that the maximum mean precipitation in the ENSO run is larger than that in the no-ENSO run, suggesting a possible influence of ENSO on the mean precipitation.

To quantify the variability of winter precipitation, Fig. 1 (right panels) also shows the standard deviation of JFM mean precipitation. In both the observations and model simulations, winter precipitation exhibits large variability over the Southeast China where the winter mean precipitation is also large (Fig. 1, left panels). The standard deviation is larger in the ENSO run (Fig. 1e) than in the no-ENSO run (Fig. 1f) and is also comparable to the observed (Fig. 1d). This clearly indicates an enhancement of winter precipitation variability in the Southeast by ENSO.

The results presented in Fig. 1 suggest that both the spatial distribution of the long-term mean and the variability of China winter precipitation are simulated reasonably well in the CFS. The overall agreement between the observed and simulated winter precipitation statistics in the ENSO run provides a basis for assessing the impact of ENSO by comparing the ENSO run and the no-ENSO run.

### 4 China winter precipitation associated with ENSO in observations

To examine the linkage between China winter precipitation and Pacific SST, an SVD analysis is performed by analyzing the covariance matrices of JFM mean precipitation in East China (100°–125°E, 22°–45°N) and JFM SST

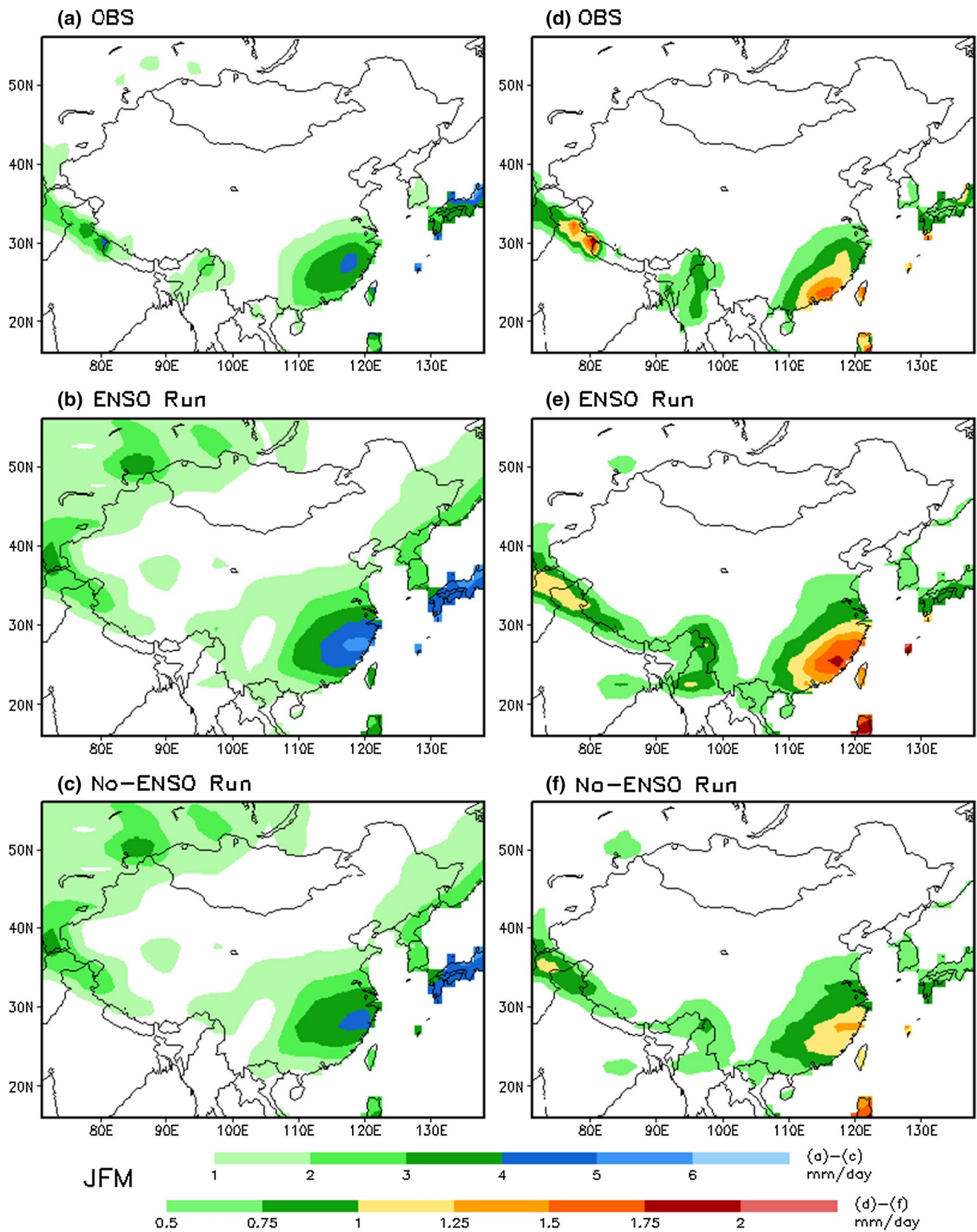
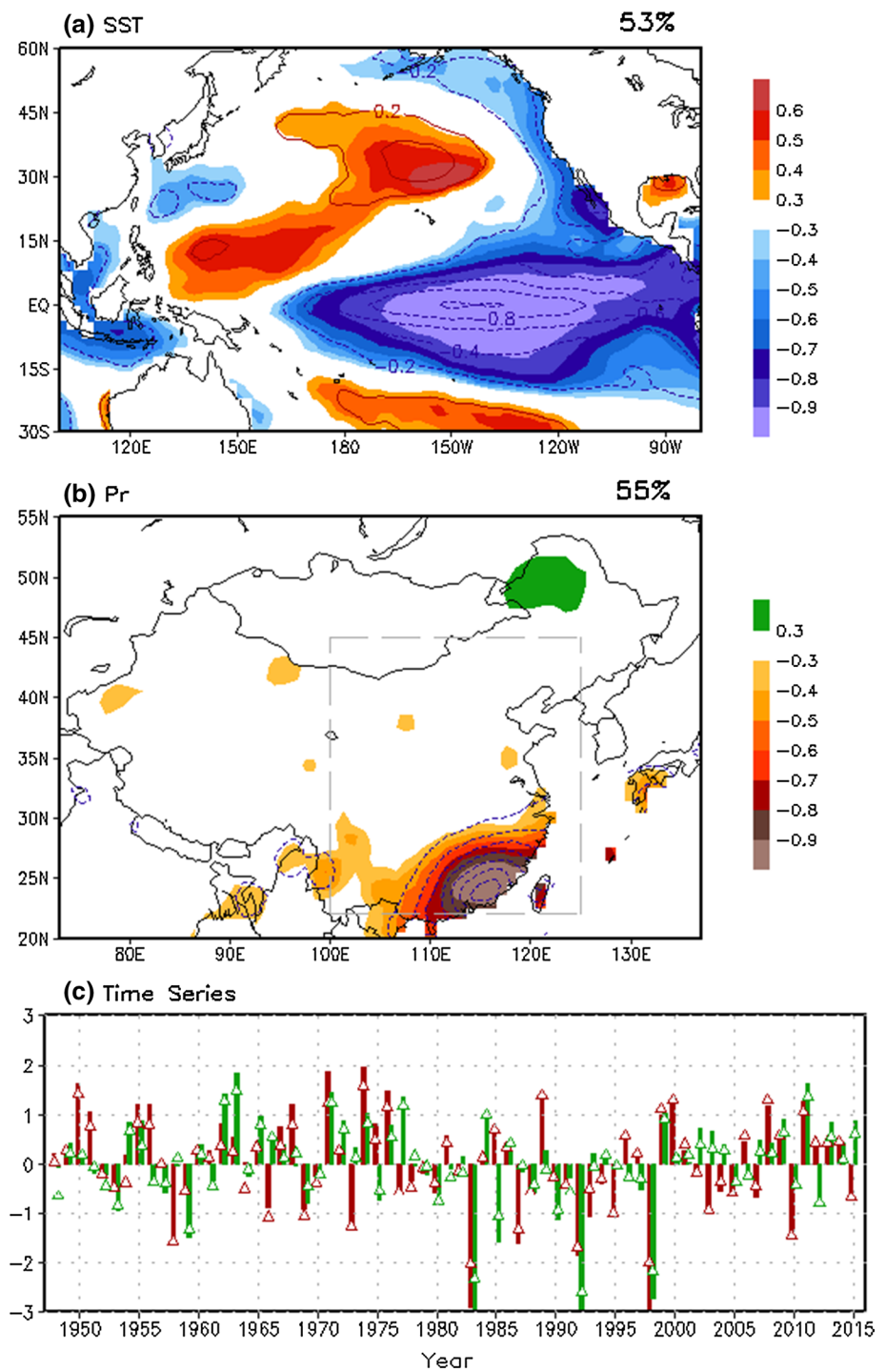


**Fig. 1** Climatology (left panels) and standard deviation (right panels) of winter (JFM) precipitation for **a, d** observations (1948–2015) and 480-year **b, e** ENSO run and **c, f** no-ENSO run. The units are  $\text{mm day}^{-1}$  for both the climatology and standard deviation of precipitation

**Fig. 2** Spatial patterns of the first SVD mode for winter (JFM) **a** Pacific SST and **b** China precipitation in the forms of homogeneous correlations (*shadings*) and regression coefficients (*contours*) against **c** their corresponding time series (*green bars* for precipitation and *red bars* for Pacific SST) based on observational data from 1948 to 2015. Contour intervals are 0.2 K in **(a)** and 0.2 mm day<sup>-1</sup> in **(b)** with negative contours *dashed*. *Shaded areas* indicate the correlations exceeding the 99% significance level. *Red triangles* in **(c)** are the negative of the Niño 3.4 SST (K) and *green triangles* are the negative of precipitation anomalies (mm day<sup>-1</sup>) averaged over Southeast China (110°–120°E, 22°–30°N)



in the tropical Pacific (120°E–70°W, 20°S–20°N) using the observational data. The spatial patterns of the first SVD mode are shown in Fig. 2a for SST and in Fig. 2b for precipitation, respectively, in the forms of homogeneous correlation (*shadings*) maps (Wallace et al. 1992) and regression coefficients (*contours*) against the corresponding SVD time series (Fig. 2c).

The first SVD mode of SST explains 53% of the total variance of winter tropical Pacific SST. The spatial pattern (Fig. 2a) is characterized by a La Niña SST distribution with large negative correlations in the eastern and central tropical Pacific, as well as negative correlations along the coast of North America. Positive correlations are found in the tropical western North Pacific and central North Pacific,

and also in the subtropical South Pacific. Associated with a one-standard-deviation fluctuation in the SVD SST time series (Fig. 2c), cold SST anomalies can be below  $-1$  K near  $150^{\circ}\text{W}$  at the equator.

The first SVD mode of precipitation (Fig. 2b) explains 55% of the total variance of winter precipitation over East China. The spatial pattern is dominated by negative correlations in the Southeast China centered at ( $115^{\circ}\text{E}$ ,  $23^{\circ}\text{N}$ ). The SVD patterns of SST and precipitation (Fig. 2a, b) suggest that during La Niña (El Niño), Southeast China winter precipitation is below (above) normal. Associated with 1-K ENSO SST anomaly in the tropical central Pacific, maximum winter precipitation anomalies can be  $1.5$  mm day $^{-1}$  in the Southeast China.

The corresponding time series for the first SVD mode of SST and precipitation are shown in Fig. 2c. The correlation between the two SVD time series is 0.57 over the 68 years. Both SST and precipitation exhibit consistent fluctuations in most winters, with cold (warm) tropical Pacific SST anomalies related to less (more) precipitation over the Southeast China. The first SVD mode accounts for 96% of the covariance between the SST and precipitation fields, suggesting a dominant role of ENSO in the co-variability between China winter precipitation and Pacific SST. Such a relationship between wintertime tropical Pacific SST and East China precipitation (Fig. 2) is consistent with previous studies (e.g., Zhang and Sumi 2002; Wu et al. 2003). In extension to previous studies, the SVD analysis presented here quantifies this relationship by the percentage of the covariance between the two fields explained by the first SVD mode and the correlation between the two SVD time series, as well as the percentage of the variance explained by this mode for the two individual fields.

In addition to the coherent interannual variations between the ENSO SST and East China precipitation, Fig. 2c also displays co-variations of ENSO and precipitation on the decadal timescale. From 1948 to 1977 both the SST and precipitation time series are largely positive, indicating more La Niña events than El Niño and more dry winters than wet winters in East China. From 1978 to 1999, in contrast, both the SST and precipitation time series are generally negative. Therefore, when there are more El Niño events than La Niña, the East China winter precipitation tends to be above normal in the second period. In the last 16 years (2000–2015), the co-variations of the ENSO SST and East China precipitation are less significant. The correlations between the two SVD time series are 0.40, 0.76, and 0.34, respectively, over the three periods, suggesting a strong association between SST and precipitation in the El Niño years and a relatively weak association in the La Niña years. The results indicate that the decadal variability of ENSO may lead to decadal variations of East China precipitation and may also modulate the strength of the

association between SST and precipitation on the decadal timescale. The weak correlation (0.34) in the most recent period (2000–2015) may be due to the weakening of the ENSO variability after 1999 (Hu et al. 2013).

The time series of both the negatives of Niño 3.4 SST and winter precipitation anomalies averaged over Southeast China ( $110^{\circ}$ – $120^{\circ}\text{E}$ ,  $22^{\circ}$ – $30^{\circ}\text{N}$ ) are superimposed on the SVD SST and precipitation time series in Fig. 2c. The regional SST and precipitation anomalies exhibit coherent fluctuations with the corresponding SVD time series with correlations of 0.971 and 0.970, respectively. The results indicate a close relationship between the ENSO SST variability and the interannual changes in Southeast China winter precipitation, which is well represented by the first SVD mode.

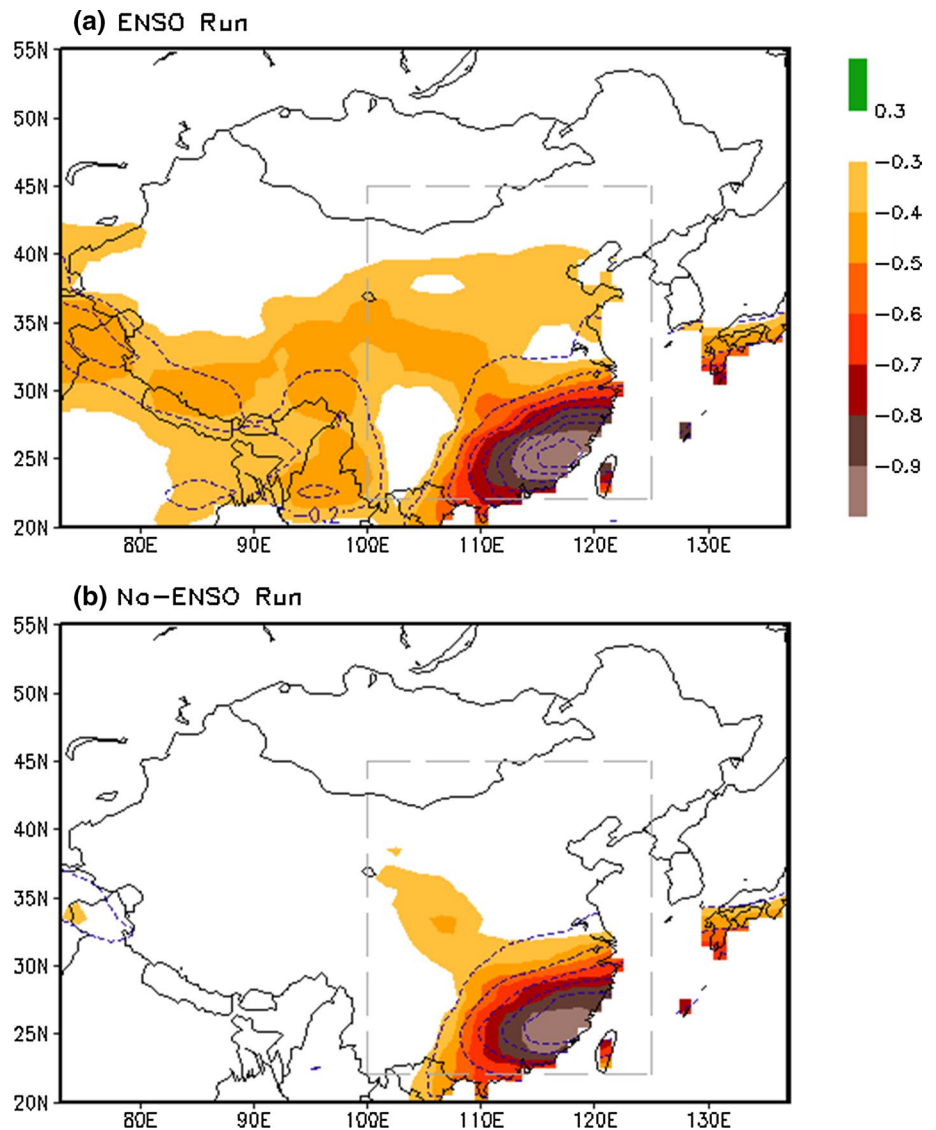
Whether the SVD mode shown in Fig. 2 represents the dominant modes of variability in the SST and precipitation fields is further examined by performing an EOF analysis for the individual SST and precipitation fields, respectively. The first EOF modes of both SST and precipitation (not shown) are almost identical to their corresponding SVD components, and explain 57 and 56% of the variance for SST and precipitation, respectively, similar to those of the SVD mode (53% for SST and 55% for precipitation). The pattern correlation between the SVD and EOF spatial patterns is 0.994 for SST and 0.997 for precipitation. The first SVD mode thus captures the co-variations of the dominant modes of the tropical Pacific SST and East China precipitation on both the interannual and interdecadal timescales.

## 5 China winter precipitation associated with ENSO in model simulations

The variability of the ENSO-related precipitation pattern is further examined for both the ENSO run and no-ENSO run. First, the model winter precipitation anomalies in East China ( $100^{\circ}$ – $125^{\circ}\text{E}$ ,  $22^{\circ}$ – $45^{\circ}\text{N}$ ) are projected onto the observed ENSO-related precipitation pattern depicted by the first SVD mode (Fig. 2b). A 480-year time series of the projection coefficients is then obtained. For the no-ENSO simulations, this time series represents the time evolution of the specific precipitation pattern similar to the observed ENSO-related one, even without the ENSO variability. The specific precipitation pattern can be reconstructed by correlating/regressing the model winter precipitation anomalies against the 480-year time series of projection coefficients for both the ENSO run and no-ENSO run, as shown in Fig. 3.

In both the ENSO run and no-ENSO run, the correlation maps (shadings in Fig. 3) display negative correlations with a center in the Southeast China, similar to that in Fig. 2b. Differences are also obvious between the two simulations. The regions of negative correlations are extended

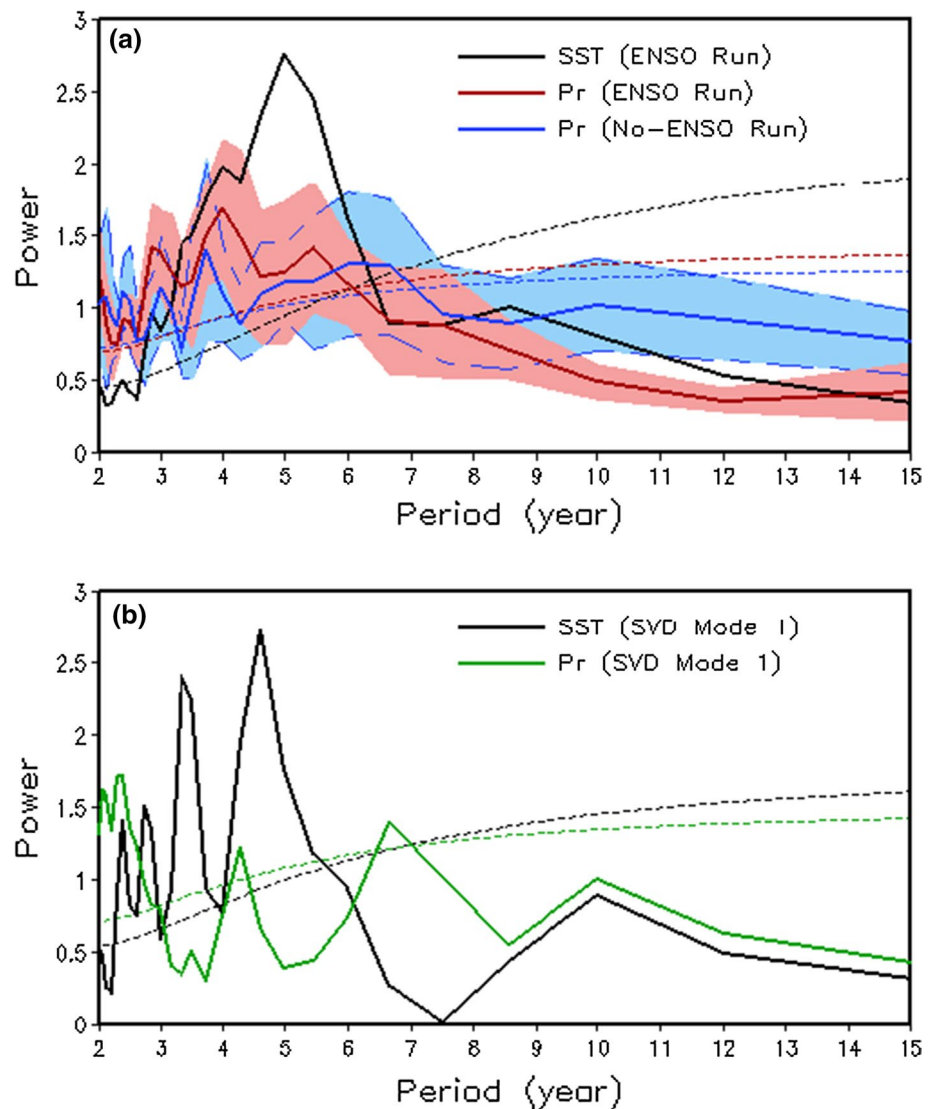
**Fig. 3** Correlation (*shading*) and regression coefficient (*contours*) of winter precipitation with the time series of the projection coefficients of model precipitation anomalies onto the observed precipitation pattern (Fig. 2b) for the 480-year **a** ENSO run and **b** no-ENSO run. Contour interval is 0.2 mm day<sup>-1</sup>. Shaded areas indicate the correlations exceed the 99% significance level



northward and westward in the ENSO run (Fig. 3a). In particular, the reconstructed precipitation anomalies (contours) are larger in the ENSO run (Fig. 3a) than in the no-ENSO run (Fig. 3b) with a roughly 50% increase in maximum precipitation anomalies ( $-16 \text{ mm day}^{-1}$  in the ENSO run vs.  $-10 \text{ mm day}^{-1}$  in the no-ENSO run). This indicates that the ENSO variability enhances the intensity of precipitation anomalies. Therefore, in the presence of ENSO, there are more winters with extreme precipitation anomalies (positive or negative) in the Southeast China. Besides the ENSO impact, there are a few other processes that also affect the winter precipitation in China, including East Asian winter monsoon, western Pacific subtropical high, and moisture transport from South China Sea and the Bay of Bengal (e.g., Cai et al. 2003; Namias 1963; Zeng et al. 2010).

The impact of ENSO on the temporal characteristics of winter precipitation is also assessed. Figure 4a shows the power spectra of the 480-year time series of the precipitation projection coefficients for both the ENSO run and no-ENSO run, as well as the Niño 3.4 SST time series in the ENSO run. Consistent with the observations, ENSO in the ENSO run is characterized by the interannual variability with significant power at 3–7 years (black line in Fig. 4a). Comparing the two simulations, winter precipitation in the ENSO run (red line in Fig. 4a) has higher power at 3–6 years than in the no-ENSO run (blue line in Fig. 4a), with three significant peaks between 3 and 6 years. To estimate whether the difference in the precipitation power spectra is distinguishable between the two runs, the 480 years are separated into 8 segments (each 60 years) to create an envelope for the spectra based on one standard

**Fig. 4** Power spectra of **a** the 480-year time series of the Niño 3.4 SST index in the ENSO run (*black*), the normalized projection coefficients of model precipitation anomalies in the ENSO run (*red*) and no-ENSO run (*blue*), respectively, and **b** the 68-year time series of the first SVD mode SST (*black*) and precipitation (*green*) in observations. *Dashed lines* are the corresponding red-noise spectra. *Pink and light blue shadings* in **(a)** denote the one-standard-deviation spreads of 8 segments of 60-year power spectra for precipitation in the ENSO run and no-ENSO run, respectively. *Long dash lines* are the envelop of the *light blue shading*



deviation of the 8-member spreads. The two peaks close to 3 and 4 years in the ENSO run are outside of the envelope of the spectra in the no-ENSO run. Thus they are well separated from the no-ENSO run. The results clearly suggest that ENSO enhances the interannual variability of winter precipitation in the Southeast. For comparison, Fig. 4b shows the power spectra of the 68-year time series of the first SVD mode SST and precipitation in observations. Overall, the peaks at the interannual timescale in the power spectra of SST and precipitation in the ENSO run are close to those in the observations.

An EOF analysis of East China winter precipitation anomalies in the no-ENSO run (not shown) exhibits the same spatial pattern as in Fig. 3b, indicating that this is also an internal mode of winter precipitation variability and can occur in the absence of ENSO variability. The results presented in Figs. 3 and 4a suggest that this internal mode is then modulated by the external ENSO forcing

with enhanced precipitation anomalies in the Southeast and strengthened variability at the interannual timescale.

## 6 Sensitivity of winter precipitation and the associated circulation responses to ENSO

### 6.1 Composite of ENSO SST for different phases and intensities

To test the sensitivity of East China winter precipitation response to different ENSO categories, such as warm phase versus cold phase, and strong events versus weak events, we have to have enough sample size for each ENSO category. The 68-year (1948–2015) observational data with limited ENSO events is clearly not appropriate for such an analysis. Given that the ENSO variability is well simulated in the ENSO run (Kim et al. 2012), the 480-year simulation



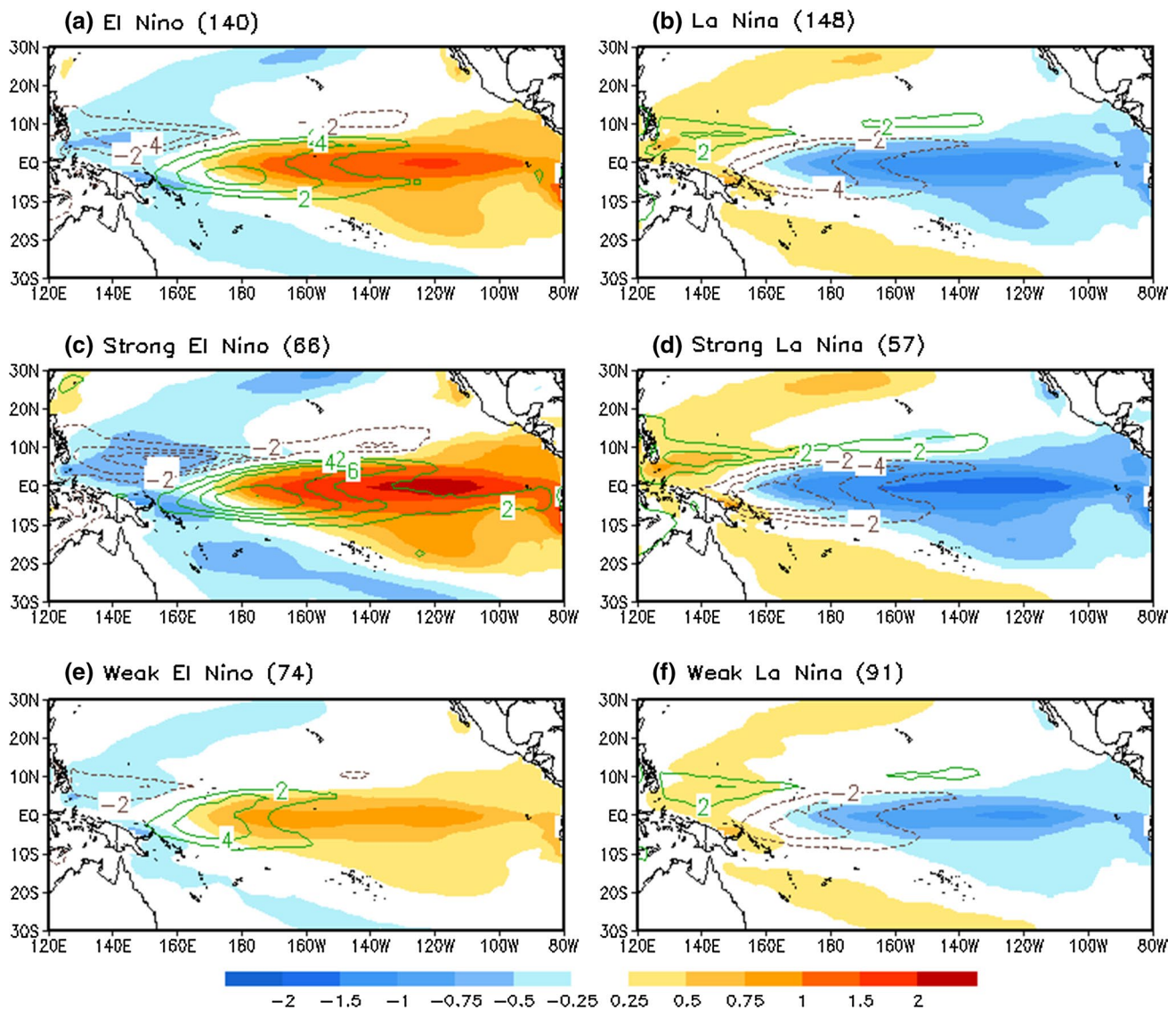


**Fig. 5** Composite of JFM seasonal mean Pacific SST anomalies (*shadings*, unit: K) and precipitation anomalies (*contours*, unit:  $\text{mm day}^{-1}$ ) for **a** all El Niño, **b** all La Niña, **c** strong El Niño, **d** strong La Niña, **e** weak El Niño, and **f** weak La Niña years in the 480-year

ENSO run. Contour interval is  $2 \text{ mm day}^{-1}$  and zero contours are omitted. The number of events for each ENSO category is listed at the top of each panel (in parentheses), which is defined by the Niño 3.4 SST index

produces a sufficient number of ENSO events and can be used for this analysis.

Similar to Wang and Kumar (2015), an El Niño (La Niña) in the ENSO simulation is defined by the JFM seasonal mean Niño 3.4 SST index with a value greater than 0.5 K (less than  $-0.5 \text{ K}$ ). All ENSO events are further categorized as strong (weak) events if the absolute value of the Niño 3.4 index is great than 1 K (between 0.5 and 1 K). With such criteria, there are 140 El Niño (148 La Niña) events in the 480-year ENSO run, among which, 66 and 74 (57 and 91) events are strong and weak El Niño (La Niña), respectively. Figure 5 shows the composite of

SST anomalies for El Niño and La Niña in the ENSO run, respectively, as well as for strong and weak events.

## 6.2 Composite of East China precipitation for different phases and intensities of ENSO

Figure 6 shows the composite of China winter precipitation anomalies in the ENSO run for different phases and intensities of ENSO. Associated with El Niño (La Niña), model precipitation in Fig. 6a (Fig. 6b) is above (below) normal in Southeast China, consistent with the SVD analysis in Fig. 2. The observed relationship between wintertime

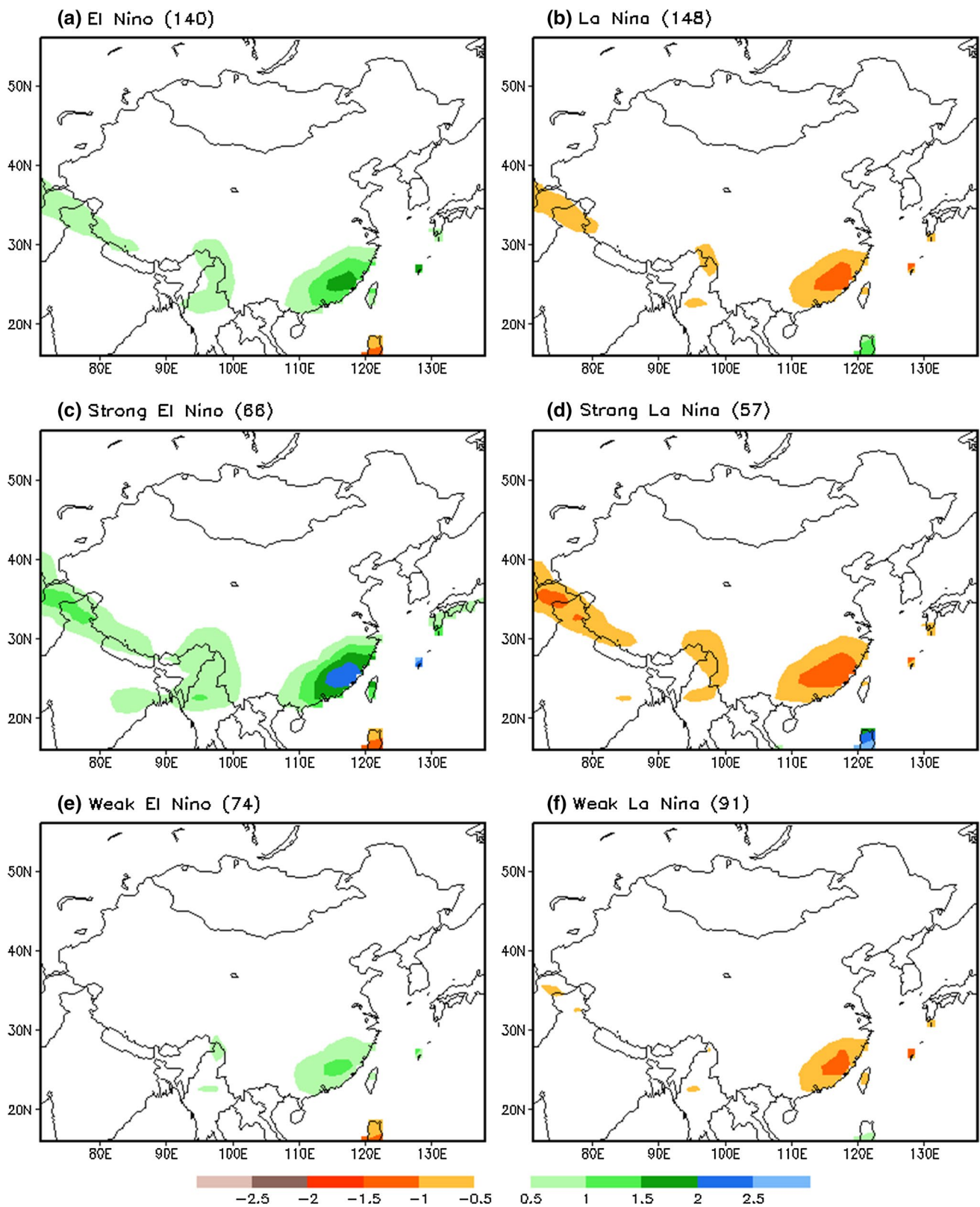


**Fig. 6** Same as Fig. 5, but for the composite of JFM seasonal mean China precipitation anomalies (unit:  $\text{mm day}^{-1}$ ) for **a** all El Niño, **b** all La Niña, **c** strong El Niño, **d** strong La Niña, **e** weak El Niño, and **f** weak La Niña years in the 480-year ENSO run

China precipitation and ENSO is thus well reproduced in the ENSO run.

Associated with the strong and weak ENSO events, there is an amplitude asymmetry in China winter precipitation anomalies between warm and cold phases (Fig. 6c–f). During El Niño, precipitation anomalies in the Southeast (Fig. 6, left panels) increase with the intensity of warm SST anomalies (Fig. 5, left panels), whereas during La Niña precipitation anomalies (Fig. 6, right panels) are less sensitive to the intensity of cold SST anomalies (Fig. 5, right panels). The results designate the nonlinearity in the amplitude of the precipitation response to ENSO.

The asymmetry of the China winter precipitation in response to El Niño and La Niña can be understood through the nonlinear relationship between anomalous tropical heating and ENSO SST. When tropical SST is warmer than 28 °C, a threshold for atmospheric deep convection (e.g., Fu et al. 1994), precipitation and associated latent heat release increase exponentially with SST because saturation vapor pressure is an exponential function of SST (Graham and Barnett 1987). However, when SST is below 28 °C, no matter how cold the SST is, no deep convection occurs in the tropics and thus no latent heat is released to the atmosphere. The nonlinear relationship is clearly illustrated by the magnitudes of precipitation anomalies associated with different ENSO categories (Fig. 5), which is a good indicator of the tropical heating for the atmosphere (Hoerling et al. 1997, 2001).

### 6.3 Sensitivity of the atmospheric circulation response to ENSO

It is the atmospheric teleconnection that links the variability of East China winter precipitation to ENSO. Therefore, we expect to see the same asymmetry in the atmospheric circulation response to El Niño and La Niña as in the precipitation response. To confirm this, Fig. 7 presents the correlations of JFM 200-hPa height anomalies from the ENSO run with the time series of projection coefficients of model precipitation onto the first SVD precipitation pattern (Fig. 2b) over the warm and cold ENSO years, and over the strong and weak ENSO years respectively, as well as over the entire 480 years for both the ENSO run and no-ENSO run.

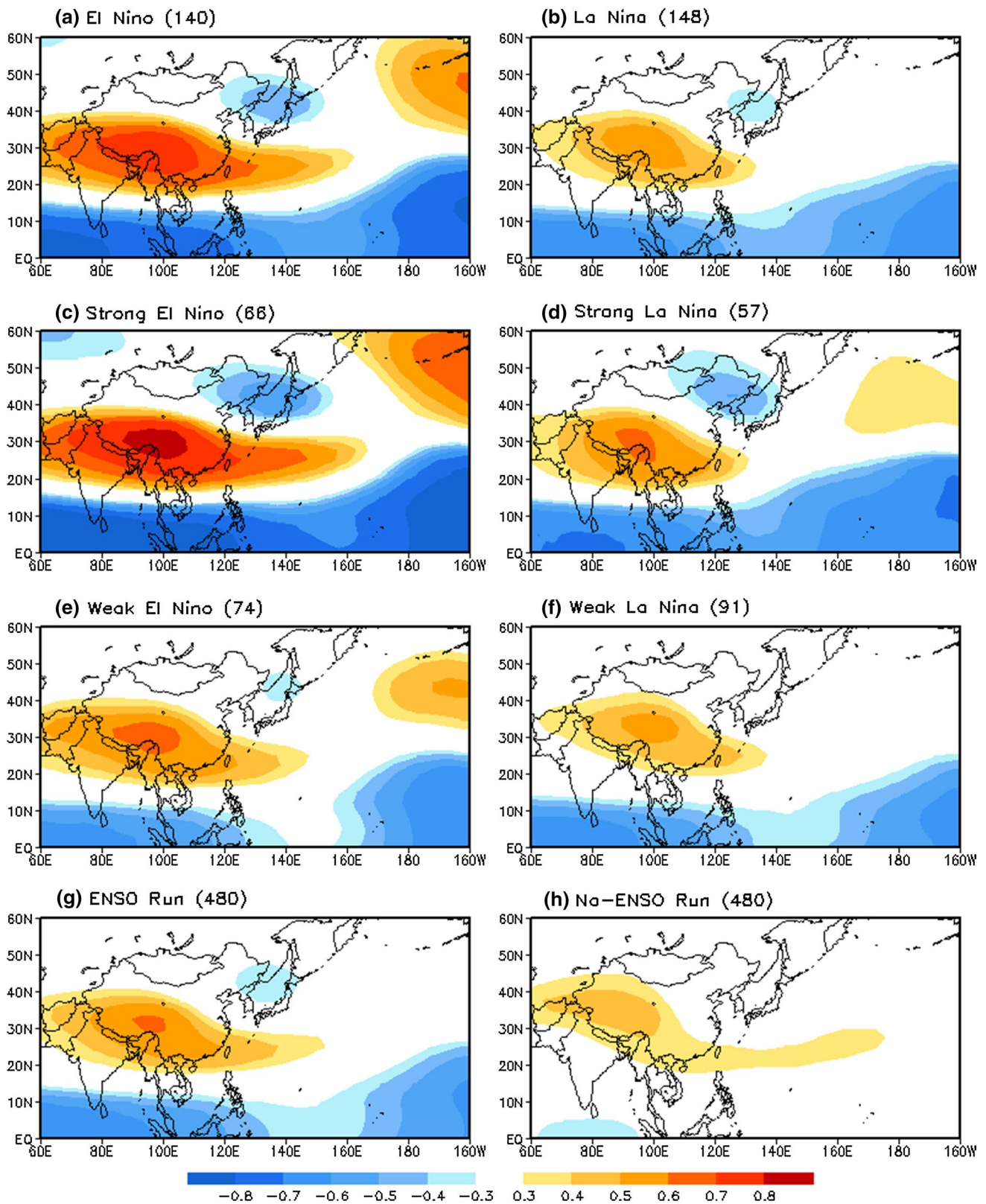
For different phases and intensities of ENSO, all correlation maps display the Pacific–East Asian teleconnection pattern (Wang et al. 2000). Associated with La Niña (Fig. 2a), winter height anomalies are below normal over the tropics and above normal over South China (Fig. 7). The circulation response is stronger in El Niño years (Fig. 7a) than in La Niña years (Fig. 7b). Consistent with the precipitation response to ENSO (Fig. 6), the circulation response is more sensitive to the intensity of El Niño (Fig. 7, left panels),

but less sensitive to the intensity of La Niña (Fig. 7, right panels). Figure 7 illustrates clearly that the strength of the link between ENSO and its forced extratropical circulation anomalies depends upon both the phase and intensity of ENSO. A comparison between Fig. 7g and h indicates that no correlations are found over the tropical Pacific in the no-ENSO run. Additionally, the correlations with the extratropical 200-hPa height are weaker in the no-ENSO run than in the ENSO run. It is also noted that in the absence of ENSO, East China precipitation mainly correlates with circulation (geopotential height) anomalies over the western China and subtropical western Pacific (Fig. 7h), which are likely associated the atmospheric internal variability. Some weak correlations are found over the tropical Indian Ocean, suggesting a link between East China precipitation and tropical Indian Ocean. In the presence of ENSO, these linkages can be significantly strengthened through the atmospheric teleconnection (Fig. 7g), which reflects the modulation of the circulation by ENSO.

### 6.4 Explanation for the observed decadal changes in the association between East China winter precipitation and tropical Pacific SST

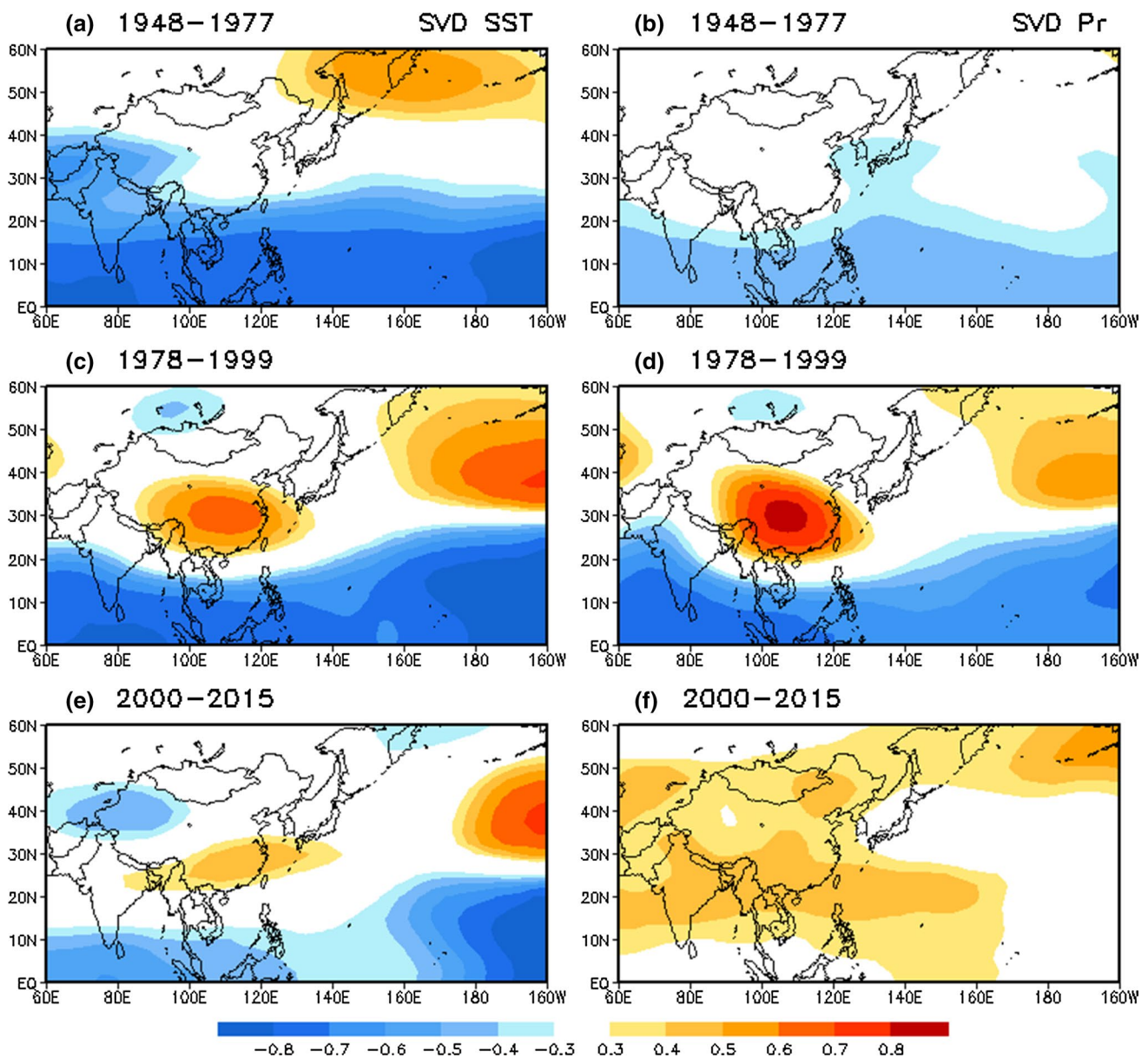
As mentioned earlier, the strength of the association between wintertime East China precipitation and tropical Pacific SST experienced decadal changes over the past 68 years (1948–2015). Quantified by the correlation between the two time series of the first SVD mode (Fig. 2c), the SST–precipitation relationship is relatively weak (0.40) over the first 30 years (1948–1977), strong (0.76) over the second 22 years (1978–1999), and weakest (0.34) over the last 16 years (2000–2015). The decadal changes in the strength of the linkage between the SST and precipitation can be explained by the sensitivity of the circulation response to ENSO.

Figure 8 shows the correlations of the observed JFM 200-hPa height anomalies with the SVD mode 1 time series of SST (left panels) and precipitation (right panels), respectively, over the three time periods. In the early period (1948–1977), there were more La Niña years than El Niño years. Therefore, the circulation response to tropical SST is expected to be weak. This is indeed the case and can be seen in Fig. 8a, b, in which signal of the teleconnection is very weak in the mid-latitudes. For the second period (1978–1999), more El Niño events occurred than La Niña. Consequently, the circulation response is strong, leading to a stronger association between China winter precipitation and tropical Pacific SST (Fig. 8c, d). In the last period, as the variability of the tropical Pacific SST became weak (Hu et al. 2013), the circulation response was also weak (Fig. 8e). As a consequence, the China winter precipitation was more likely influenced by the factors other than the



**Fig. 7** Correlation of JFM 200-hPa height anomalies with the time series of projection coefficients of JFM model precipitation onto the SVD1 precipitation pattern for **a** all El Niño, **b** all La Niña, **c** strong El Niño, **d** strong La Niña, **e** weak El Niño, **f** weak La Niña, and **g**

all years in the 480-year ENSO run, as well as **h** all years in the no-ENSO run. Shaded areas indicate the correlations above the 95% significance level



**Fig. 8** Correlation of JFM 200-hPa height anomalies with the first SVD time series of SST (*left panels*) and precipitation (*right panels*), respectively, for the periods of **a** 1948–1977, **b** 1978–1999, and **c** 2000–2015. *Shaded areas* indicate the correlations above the 95% significance level

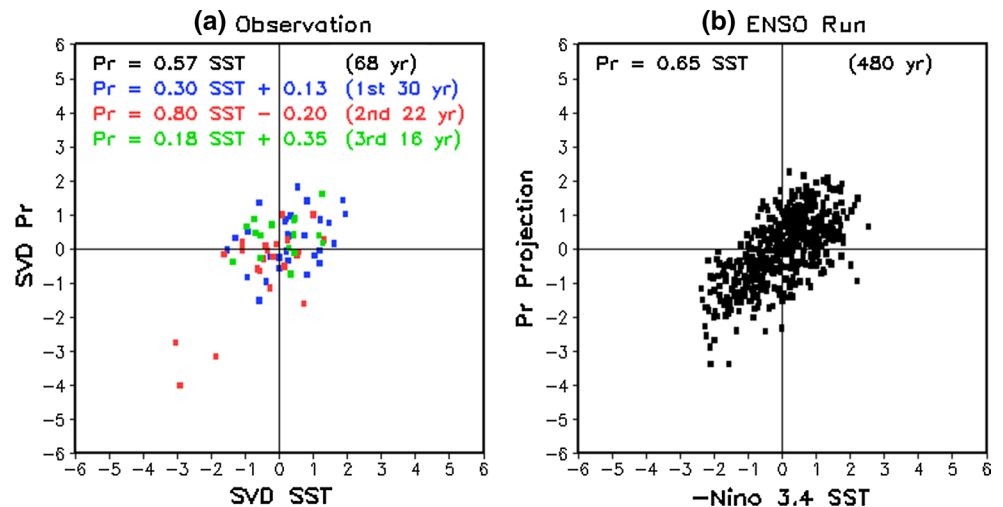
tropical SST forcing, which is manifested by the large differences between the circulation patterns in Fig. 8e, f. As a result, the correlation between the SVD SST and precipitation time series is weakest in the last period.

The results presented here suggest that the decadal modulation of East China winter precipitation by ENSO can be interpreted in two aspects. First, on an interannual timescale, above-normal (below-normal) precipitation anomalies in Southeast China are generally associated with El Niño (La Niña). The decadal variations of ENSO (i.e., more La Niña years during 1948–1977 and more El Niño years during 1978–1999) then lead to decadal variations in

East China precipitation with overall drier winters in the earlier period and overall wetter winters in the latter period. Second, the extratropical circulation response to ENSO is sensitive to both the phase and intensity of ENSO. This sensitivity together with the decadal variations of ENSO results in the decadal changes in the strength of the association between wintertime tropical Pacific SST and East China precipitation.

Figure 9a shows the scatter plot of SVD mode 1 SST time series versus precipitation time series for observations over the three periods (1948–1977, 1978–1999, and 2000–2015). The linear regression equations for the three periods are also

**Fig. 9** Scatter plots of (a) SVD mode 1 SST versus SVD mode 1 precipitation time series with observational data for the first 30 years (1948–1977, *blue*), the second 22 years (1978–1999, *red*), and the third 16 years (2000–2015, *green*), and (b) the negative of normalized Niño 3.4 SST time series versus SVD mode 1 precipitation projection coefficients in the 480-year ENSO run. The linear regression equation for each period is also listed



provided. The magnitude of regression coefficients indicates the strength of the link between tropical SST and East China precipitation, with values of 0.30, 0.80, and 0.18, respectively, for the three period. Figure 9b shows the scatter plot of the 480-year normalized Niño 3.4 SST index versus SVD mode 1 precipitation projection coefficients in the ENSO run. The regression coefficient (0.65) for the 480-year ENSO run is close to that (0.57) of the 68-year observations.

Previous studies also suggested that the ENSO impact on China precipitation can be modulated by the Pacific decadal oscillation (PDO; Mantua et al. 1997). For example, Wang and Li (2015) demonstrated that when the PDO is in a positive phase, the precipitation in Southern China is significantly enhanced during El Niño, but it has no significant change during La Niña. However, when the PDO is in a negative phase, the precipitation in Southern China is significantly reduced during La Niña, whereas the increase in precipitation during El Niño is only a half of that with a positive PDO phase.

## 7 Conclusions

In this study the relationship between wintertime tropical Pacific SST and East China precipitation was assessed using both 68-year observational data and two 480-year CFS coupled model simulations with and without ENSO. The observational analysis with the SVD method suggests coherent variations between ENSO SST and Southeast China precipitation on both interannual and decadal timescales. On the interannual timescale, Southeast China pluvial (drought) tends to be associated with El Niño (La Niña). On the decadal timescale, there are close relationships between more La Niña (El Niño) events and overall drier-than-normal (wetter-than-normal) winters in Southeast China during 1948–1977 (1978–1999). In the most recent

years (2000–2015) the relationship between East China precipitation and tropical Pacific SST is relatively weak.

A comparison between the ENSO run and no-ENSO run indicates that ENSO not only enhances the amplitude of East China precipitation anomalies but also changes the frequency of the precipitation variability. In the presence of ENSO, maximum precipitation anomalies over Southeast China can be increased by 50%. Moreover, the peaks of the power spectrum of the precipitation also shifts from higher frequencies to the interannual timescale (3–6 years).

A further analysis of the ENSO run discloses a sensitivity of East China precipitation and the associated circulation responses to ENSO. The precipitation and circulation anomalies increase with the ENSO SST anomalies during El Niño, but they are less sensitive to the SST anomalies during La Niña. Given the decadal changes in both the occurrence frequency and intensity of El Niño and La Niña, the asymmetry between the responses to warm and cold phases of ENSO helps understand the observed decadal changes in the strength of the association between East China precipitation and tropical Pacific SST.

**Acknowledgements** The authors would like to thank two anonymous reviewers and the editor for their insightful and constructive comments and suggestions. This study was supported by the China Special Fund for Meteorological Research in the Public Interest (Major project, Grant GYHY201506001), the National Natural Science Foundation of China (Grant 41275092), the Sino-US Center for Weather and Climate Extremes (CWCE) at Nanjing University of Information Science and Technology, and the Priority Academic Program Development of Jiangsu Higher Education Institutions (PAPD).

## References

- Bretherton CS, Smith C, Wallace JM (1992) An intercomparison of methods for finding coupled patterns in climate data. *J Clim* 5:541–560

- Cai X, Wen Z, Wu B (2003) The relationship between the western Pacific subtropical high and ENSO and its influence on rainfall distribution of rainy season in Fujian. *J Trop Meteorol* 19:36–42
- Chen M, Xie P, Janowiak JE, Arkin PA (2002) Global land precipitation: a 50-year monthly analysis based on gauge observations. *J Hydrometeorol* 3:249–266
- Chen L, Zhou X, Li W (2004) Characteristics and formation mechanism of climate change in China in recent 80 years. *J Meteorol* 62:634–646 (in Chinese)
- Chen GJ, Wei FY, Gong YF (2010) Assessing the extended range forecast error of NCEP/CFS in the summer of East Asia. *J Appl Meteorol Sci* 21:659–670 (in Chinese)
- Chen Y, Zhao Y, Feng J, Wang F (2012) ENSO cycle and climate anomaly in China. *Chin J Oceanol Limnol* 30:985–1000
- Feng S, Hu Q (2004) Variations in the teleconnection of ENSO and summer rainfall in Northern China: a role of the Indian summer monsoon. *J Clim* 17:4871–4881
- Feng P, Li C, Li X (1985) Analysis of major meteorological disasters in China (1951–1980). Meteorology Press, Beijing, p 273 (in Chinese)
- Fu R, Del Genio AD, Rossow WB (1994) Influence of ocean surface conditions on atmospheric vertical thermodynamic structure and deep convection. *J Clim* 7:1092–1108
- Gao H et al (2008) Analysis of the severe cold surge, ice-snow and frozen disasters in South China during January 2008: II. Possible climate causes. *Meteorol Mon* 34:101–106 (in Chinese)
- Graham NE, Barnett TP (1987) Observations of sea surface temperature and convection over tropical oceans. *Science* 238:657–659
- He S, Wang H, Liu J (2013) Changes in the relationship between ENSO and Asia-Pacific midlatitude winter atmospheric circulation. *J Clim* 26:3377–3393
- Hoerling MP, Kumar A, Zhong M (1997) El Niño, La Niña, and the nonlinearity of their teleconnections. *J Clim* 10:1769–1786
- Hoerling MP, Kumar A, Xu T (2001) Robustness of the nonlinear climate response to ENSO's extreme phases. *J Clim* 14:1277–1293
- Hu Z-Z, Kumar A, Ren H-L, Wang H, L'Heureux M, Jin F-F (2013) Weakened interannual variability in the tropical Pacific Ocean since 2000. *J Clim* 26:2601–2613
- Jin Z, Tao S (1999) A study on the relationships between ENSO cycle and rainfalls during summer and winter in eastern China. *Chin J Atmos Sci* 23:663–672 (in Chinese)
- Kalnay E et al (1996) The NCEP–NCAR 40-year reanalysis project. *Bull Am Meteorol Soc* 77:437–471
- Kim ST, Yu J-Y, Kumar A, Wang H (2012) Examination of the two types of ENSO in the NCEP CFS model and its extratropical associations. *Mon Weather Rev* 140:1908–1923
- Kumar A, Hoerling MP (2003) The nature and causes for the delayed atmospheric response to El Niño. *J Clim* 16:1391–1403
- Kumar A, Wang H, Wang W, Xue Y, Hu Z-Z (2013) Does knowing the oceanic PDO phase help predict the atmospheric anomalies in subsequent months? *J Clim* 26:1268–1285
- Li C, He J, Zhu J (2004) A review of decadal/interdecadal climate variation studies in China. *Adv Atmos Sci* 21:425–436
- Mantua NJ, Hare SR, Zhang Y, Wallace JM, Francis RC (1997) A Pacific interdecadal climate oscillation with impacts on salmon production. *Bull Am Meteorol Soc* 78:1069–1079
- Moorthi S, Pan H-L, Caplan P (2001) Changes to the 2001 NCEP operational MRF/AVN global analysis/forecast system. NWS Tech Proced Bull. 484:14 <http://www.nws.noaa.gov/om/tpb/484.htm>
- Namias J (1963) Large-scale air-sea interactions over the North Pacific from summer 1962 through the subsequent winter. *J Geophys Res: Atmos* 68:6171–6186
- Pacanowski RC, Griffies SM (1998) MOM 3.0 manual. NOAA/Geophysical Fluid Dynamics Laboratory, Princeton, p 668
- Saha S et al (2006) The NCEP climate forecast system. *J Clim* 19:3483–3517
- Smith TM, Reynolds RW, Peterson TC, Lawrimore J (2008) Improvements to NOAA's historical merged land-ocean surface temperature analysis (1880–2006). *J Clim* 21:2283–2296
- Snedecor GW, Cochran WG (1989) Statistical methods, 8th edn. Iowa State University Press, Ames, p 503
- Wallace JM, Smith C, Bretherton CS (1992) Singular value decomposition of wintertime sea surface temperature and 500-mb height anomalies. *J Clim* 5:561–576
- Wang H, Fu R (2000) Winter monthly mean atmospheric anomalies over the North Pacific and North America associated with El Niño SSTs. *J Clim* 13:3435–3447
- Wang H, Kumar A (2015) Assessing the impact of ENSO on drought in the US Southwest with NCEP climate model simulations. *J Hydro* 526:30–41
- Wang J, Li C (2015) The possible influence of the PDO on the ENSO and Southern China winter rainfall. *J Ocean Univ China: Nat Sci Ed* 45:1–9
- Wang B, Wu R, Fu X (2000) Pacific-East Asian teleconnection: How does ENSO affect East Asian climate? *J Clim* 13:1517–1536
- Wang L et al (2008) Analysis of the severe cold surge, ice-snow and frozen disasters in South China during January 2008: I. Climatic features and its impact. *Meteorol Mon* 34:95–100 (in Chinese)
- Wang H, Kumar A, Wang W, Xue Y (2012a) Seasonality of the Pacific decadal oscillation. *J Clim* 25:25–38
- Wang H, Kumar A, Wang W, Xue Y (2012b) Influence of ENSO on Pacific decadal variability: an analysis based on the NCEP climate forecast system. *J Clim* 25:6136–6151
- Wang H, Murtugudde R, Kumar A (2016) Evolution of Indian Ocean dipole and its forcing mechanisms in the absence of ENSO. *Clim Dyns* 47:2481–2500
- Wu R, Hu Z-Z, Kirtman BP (2003) Evolution of ENSO-related rainfall anomalies in East Asia and the processes. *J Clim* 16:3741–3757
- Yang S, Zhang Z, Kousky VE, Higgins RW, Yoo SH, Liang J (2008) Simulations and seasonal prediction of the Asian summer monsoon in the NCEP Climate Forecast System. *J Clim* 21:3755–3775
- Ye Y (1988) Relations between ENSO events and precipitation in the Yangtze River basin during flood season. *Meteorol Mon* 14:42–44 (in Chinese)
- Yuan Y, Li C, Yang S (2014) Decadal anomalies of winter precipitation over southern China in association with El Niño and La Niña. *J Meteorol Res* 28:91–110
- Zeng J, Zhang Q, Wang T (2010) Analysis of the relationship between East Asian winter monsoon and winter precipitation in southern China. *Plateau Meteorol* 29:975–981
- Zhang RH, Sumi A (2002) Moisture circulation over East Asia during El Niño episode in northern winter, spring and autumn. *J Meteorol Soc Jpn* 80:213–227
- Zhou L, Tam CY, Zhou W, Chan JCL (2010) Influence of South China Sea SST and the ENSO on winter rainfall over South China. *Adv Atmos Sci* 27:832–844
- Zong H, Chen L, Zhang Q (2010) The instability of the interannual relationship between ENSO and the summer rainfall in China. *Chin J Atmos Sci* 34:184–192 (in Chinese)